npj | 2D Materials and Applications

www.nature.com/npj2dmaterials

REVIEW ARTICLE OPEN

Emerging nanofabrication and quantum confinement techniques for 2D materials beyond graphene

Michael G. Stanford[1], Philip D. Rack[1,2] and Deep Jariwala[3]

Recent advances in growth techniques have enabled the synthesis of high-quality large area films of 2D materials beyond graphene. As a result, nanofabrication methods must be developed for high-resolution and precise processing of these atomically thin materials. These developments are critical both for the integration of 2D materials in complex, integrated circuitry, as well as the creation of sub-wavelength and quantum-confined nanostructures and devices which allow the study of novel physical phenomena. In this review, we summarize recent advances in post-synthesis nanopatterning and nanofabrication techniques of 2D materials which include (1) etching techniques, (2) atomic modification, and (3) emerging nanopatterning techniques. We detail novel phenomena and devices which have been enabled by the recent advancement in nanofabrication techniques and comment on future outlook of 2D materials beyond graphene.

npj 2D Materials and Applications (2018)2:20 ; doi:10.1038/s41699-018-0065-3

INTRODUCTION

Semiconductor electronics and opto-electronics is a high volume, scaled-up, and commercial technology. Precise dimensional and compositional control in silicon over nm^2 device areas combined with availability of silicon in large quantities with high crystalline quality has been the key to success and prevalence of silicon-based electronics. While silicon continues to play a dominant role in microelectronics, it is approaching its fundamental limits in terms of scaling down as well as device performance.[1,2] Therefore, new materials are constantly being sought, discovered, and researched to either supplement or replace silicon in electronic devices. Several such materials have been heavily investigated over the past two decades ranging from individual organic molecules and polymers[3,4] to carbon nanotubes[5–7] and semiconducting nanowires.[8,9] However, the requirement of uniform, electronically homogeneous and structurally monodisperse material precludes most contenders to replace silicon. Toward that end, the isolation of graphene and measurement of its electrical properties presented a landmark moment for materials, devices, and condensed matter physics research.[10–12] However, graphene is semi-metallic in nature and therefore unsuitable for electronic-switching devices. Soon thereafter, multiple other layered crystals were identified and isolated into single-unit cell thick monolayers. Among them, the layered mono and dichalcogenides, nitrides and oxides as well as the elemental layered allotrope of phosphorus were identified to have semiconducting or insulating character and therefore presented a unique opportunity for two-dimensional (2D) opto-electronics.[13–18]

However, the isolation and identification of a novel semiconductor is only the starting point relative to commercial scale applications. Uniform and large area synthesis and, more importantly, amenability to nanofabrication techniques for spatial modulation of composition, carrier concentration (doping), and morphology is critical for advanced applications and bench marking with known, commercialized semiconductors such as Si and III-V semiconductors. Toward that end, significant progress has been achieved for the case of post-graphene 2D materials over the past few years. With that said, we note that an overwhelming number of reviews are already available on the growth, synthesis, physical and chemical properties, as well as device advancements resulting from post-graphene 2D materials.[1,19–29] Therefore, in this review, we specifically attempt to summarize the progress in spatially controlled, structural modulation from the perspective of applications in electronic and opto-electronic devices. Specifically, we focus on transition metal dichalcogenides (TMDCs), and to a lesser extent MXenes and black phosphorus (BP) on the materials side and further focus on advancements in nanoscale etching, doping, phase and defect patterning techniques to induce new structures or fundamental physical phenomena for unique advantages or advancements in terms of device properties.

Based on the above overview, this review is divided into four distinct sections. The first three sections are dedicated to (1) etching, (2) atomic modification including phase, defect and dopant patterning, and (3) new techniques for lithographic patterning and growth including controlled growth of hetero-structures and doping. The last section is dedicated to novel fundamental physical phenomena and device applications that hold promise for the future based on nanoscale spatial modulation of the structure in these 2D materials.

As the chemical nature of the of the aforementioned materials (TMDCs, MXenes, and BP) are relevant toward understanding many of the processing techniques detailed in this review, a brief summary with relevant references is provided. Common among the materials discussed is the fact that these are 2D layered materials, in which the layers are weakly held together by van der Waals interactions. (1) TMDCs chemical formula can be generalized as MX_2, where M is a transition metal of group 4–10, and X is

[1]Department of Materials Science and Engineering, University of Tennessee, Knoxville, TN 37996, USA; [2]Center for Nanophase Materials Sciences, Oak Ridge National Laboratory, Oak Ridge, TN 37831, USA and [3]Department of Electrical and Systems Engineering, University of Pennsylvania, Philadelphia, PA 19104, USA
Correspondence: Philip D. Rack (prack@utk.edu) or Deep Jariwala (dmj@seas.upenn.edu)

Received: 30 March 2018 Revised: 9 June 2018 Accepted: 11 June 2018
Published online: 16 July 2018

a chalcogen species. Chalcogens include S, Se, and Te, therefore giving a large variety of TMDCs which can be synthesized. TMDCs which are formed of group 4–7 transition metals (which will be discussed in this review) form layered structures which consist of hexagonally packed metal atoms which are sandwiched between two layers of chalcogen atoms. The coordination of the metal atoms varies depending upon the phase of the material, but is typically trigonal prismatic coordination for the semiconducting phase of commonly studied TMDCs such as MoS_2 and WS_2 (other phases will be discussed where relevant in this review). A comprehensive review of the chemistry of TMDCs can be found in ref. [28] (2) MXenes are formed from a 3D material consisting of a layered MAX structure, where M is a transition metal, A is a group III or IV element, and X is carbon or nitrogen. To form MXenes, the "A" layer is etched away leaving the MXene with a general structure of $M_{n+1}X_nT_x$ ($n = 1$–3), where T_x is the surface termination which can be hydroxyl, oxygen or fluorine, for example.[30] From the general formula, MXenes are generally 2D metal carbides with various surface termination. Some example materials include Ti_2CT_x, $Ti_3C_2T_x$, and $Nb_4C_3T_x$. This relatively new class of materials offers a vast amount of novel 2D materials, owing to the large combinations of transition metals and surface terminations that can be combined. MXene are generally unstable in atmosphere as they are prone to oxidation.[31] A comprehensive review can be found in ref. [30] (3) BP is a single element 2D material composed of solely phosphorus atoms. Semiconducting BP has a puckered orthorhombic structure, in which the P has two atomic layers with two different bond lengths. A 0.2224 nm bond connects P atoms in the same plane, whereas a 0.2244 nm bond connects P atoms out of plane. Top view of the 2D BP shows a hexagonal structure with bond angles of 102.1° and 96.3°. Similar to MXenes, BP is not stable in atmosphere due to oxidation. A comprehensive review on BP can be found in ref. [18]

ETCHING

Patterning 2D materials is critical for their incorporation into integrated circuitry as well as the general fabrication of nanostructures. Patterning by chemical etching processes has enabled the fabrication of various forms of complex circuitry and logic gates.[32,33] For example, Fig. 1a shows the first fully functional microprocessor created from 2D semiconductors that was fabricated by patterning large-area MoS_2.[34] For implementation of 2D materials in circuitry, etch processes should be compatible with common device materials and highly controllable. In fact, the efficiency of the etching method is not critical due to the atomic thickness of 2D materials. Instead, it is more critical to be able to pattern with high resolution without altering physical, electronic, and optical properties of the remaining film. Etch processes are needed for complete material removal, as well as controlled thinning in a layer-by-layer manner. Popular chemical etching processes can be generally grouped into the following categories: (1) wet chemical, (2) reactive gas-assisted, (3) plasma/reactive ion, and (4) atomic layer etching (ALE).

Wet etching

Wet etches are carried out by submerging the targeted material in a liquid solution for a prescribed amount of time. The etchant solution typically forms a compound with the targeted material, which subsequently dissolves in the solution. Etch efficiencies are controlled by changing etchant solution concentration as well as temperature. Wet etches have commonly been used in the synthesis of MXenes. In this process, the etchant is used to selectively remove the "A" species from a MAX phase material, yielding MXenes.[30] Wet etching processes have also been used in patterning TMDCs. Metal-assisted chemical etching has been demonstrated by depositing Al on top of MoS_2 and then etching with tetramethylammonium hydroxide to selectively remove the Al and the underlying TMDC.[35] In general, very high etch yields can be achieved with wet etch processes, but with little control over atomic layer removal and a high degree of isotropic etching. Therefore, wet etching is most useful for nanopatterning by complete material removal and not atomic layer removal.

Reactive gas-assisted etching

Similarly, various reactive gas-assisted processes have been developed to etch 2D materials in an isotropic manner. These are relatively high-pressure processing techniques which are best suited for large area material removal. It has been demonstrated that XeF_2 at a pressure of ~1–3 torr can be used to spontaneously etch MoS_2 at room temperature.[36,37] In general, the family of halogenated gases are attractive candidates for the spontaneous etching of 2D materials. Oxidation has also been demonstrated to etch various 2D materials via annealing in air,[38] Ar-O_2 flow,[39] and water steam[40] to name a few. Reactive gas etching should be most useful for complete material removal and not atomic layer thinning, because non-volatile partial reaction by-products can significantly alter or degrade material properties.

Plasma and reactive ion etching (RIE)

Plasma and reactive ion dry etching processes offer some key advantages over wet etches and spontaneous reactive-gas etches. During typical plasma etching processes, a plasma is generated with a gas species in close proximity to (either direct or remote) the material which is to be etched. Radicals or ions in the plasma generate volatile etch compounds with the targeted material resulting in material removal. RIE systems typically allow good control over processing conditions such as plasma density, pressure, temperature, and etch time, which has made RIE a popular etching technique for processing 2D materials. Additionally, RIE processes are largely anisotropic in nature. Some popular plasma species for etching TMDCs include O_2,[41–44] CF_4,[41,45] and SF_6.[46] Fluorinated plasma species (and other halogen species) are popular etching plasmas due to their high electronegatively. Therefore, many elements form compounds with fluorine which are volatile at room temperature. Alternatively, oxygen plasma can be used to generate volatile species with some 2D materials. Oxygen plasma generating instruments are also abundant, as they are commonly used to clean surfaces contaminated with hydrocarbons. However, when used to thin 2D materials, plasma etching processes can result in the undesired inclusion of etchant species in the target material.[43] Figure 1b demonstrates that after O_2 plasma etching, a Mo^{6+} $3d_{3/2}$ peak is observed in XPS measurements, which indicates partial oxidation. Similar observations have been made when etched with fluorinated or chlorinated plasmas,[47] thus emphasizing the need for post-etching procedures to eliminate residual contaminants and defects. Figure 1c shows a re-sulfurization process which was developed to heal MoS_2 films after O_2 plasma etching. XPS data (Fig. 1b) suggests that re-sulfurization reduced undesired oxidation in the etched MoS_2. However, even small quantities of residual defects or dopant atoms remaining after etch processes can significantly alter electronic properties.

Atomic layer etching

Perhaps most promising for the precise patterning and thinning of 2D materials are ALE techniques. These processes enable the controlled removal of monolayers (or sub-monolayers) and typically rely on self-limiting half-reactions. Half-reactions can be thermal processes, chemical reactions, plasma exposures, or ion irradiation to name a few. Therefore, there are many permutations of ALE processes which can be developed for various materials and applications. Figure 1d demonstrates an ALE technique used

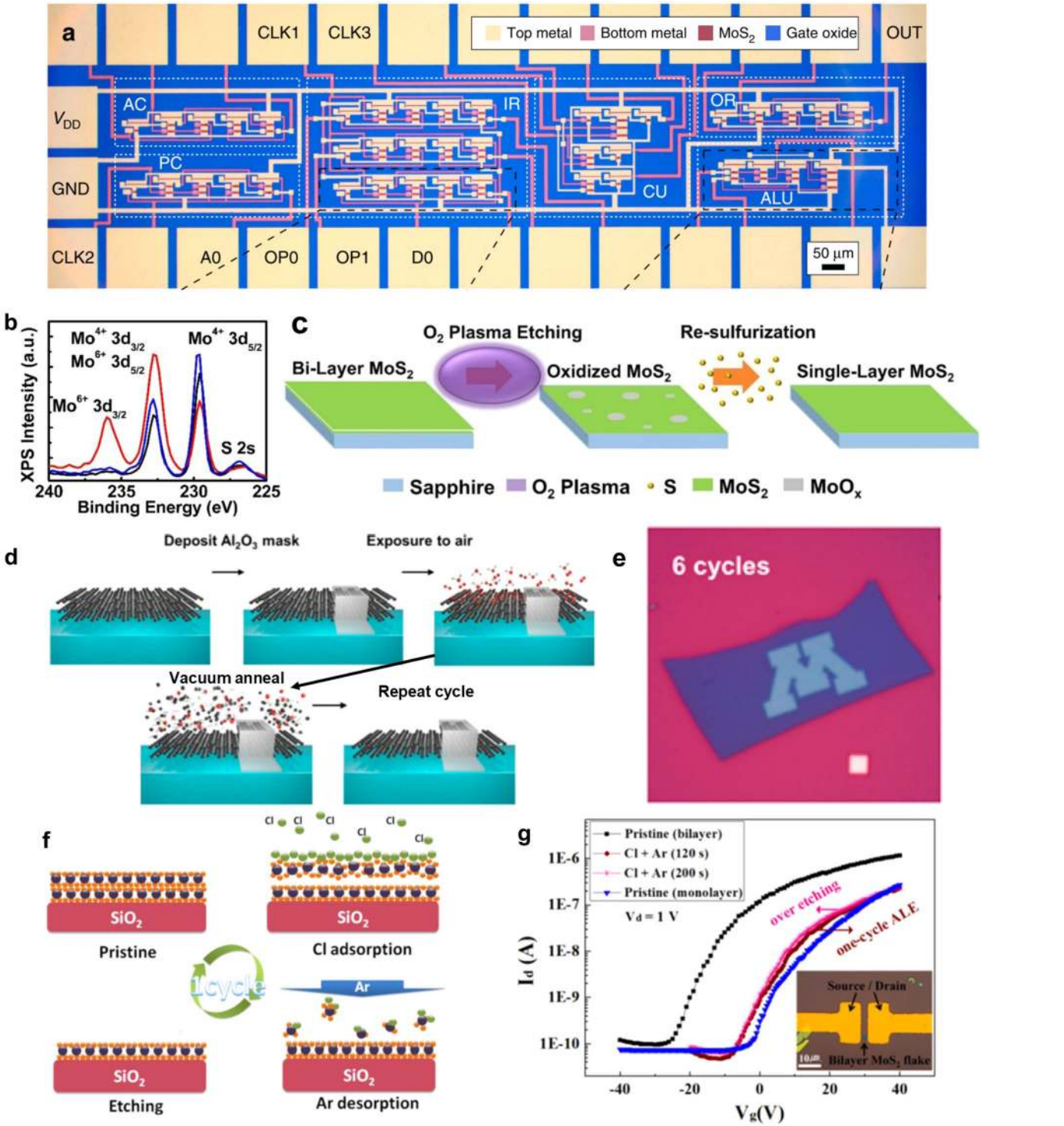

Fig. 1 Etching. **a** Microscope image of a microprocessor fabrication with an MoS_2 active layer. Scale bar is 50 mm (reprinted from ref. [34]). **b** The XPS curves of a MoS_2 sample with 10 s oxygen plasma treatment before (red line) and after (blue line) the re-sulfurization procedure. The XPS curve of the as-grown sample (black line) is also shown in the figure. **c** A schematic diagram showing the layered removal and healing procedures of MoS_2 through the oxygen plasma treatment and a subsequent re-sulfurization procedure (reprinted with permission from ref. [43] ©2017 IOP Publishing). **d** Cartoon representation detailing each important step in one cycle of the cyclic oxidation/annealing process of black phosphorous. **e** Optical micrograph of the sample after six thinning cycles. The M logo region is passivated with Al_2O_3 and the other flake regions are thinned in a cyclical manner (adapted with permission from ref. [48] Copyright 2017 American Chemical Society). **f** Schematic drawing of MoS_2 ALE cycle for the layer-by-layer etching (reprinted with permission from ref. [47] Copyright 2015 American Chemical Society). **g** Transfer curves of the bottom-gate MoS_2 field-effect transistors (FETs) that were fabricated with exfoliated bilayer MoS_2, the exfoliated monolayer MoS_2, and the exfoliated bilayer MoS_2 after one cycle of MoS_2 ALE with 120 s (monolayer etching condition) and 200 s of Ar^+ exposure (reprinted with permission from ref. [49] Copyright 2017 American Chemical Society)

for the atomic layer removal of black phosphorous.[48] In this process, the first half-reaction exposes the BP to air. This self-terminating process results in the oxidation of the top monolayer. During the second half-reaction, the material is vacuum annealed which results in the sublimation of the oxidized phosphorus layer. This process can be used to thin or pattern the BP in a controlled manner as demonstrated in Fig. 1e. An ALE process used to etch MoS_2 is also shown in Fig. 1f.[47] Chlorine radicals were adsorbed to the surface in a first half-reaction and the chlorinated MoS_2 was bombarded by a low energy Ar^+ beam to promote desorption for the second half-reaction. By tuning ion bombardment dose, the residual Cl can be completely reduced.[49] This enables the controlled thinning of MoS_2 free of unintended dopants from the etching process, as confirmed by high-quality FETs (Fig. 1g). Various other ALE studies have achieved controlled layer-by-layer etching.[44,50]

Much of the literature for controlled thinning of 2D materials pertaining to ALE omit transport characterization of the resultant material. In fact, energetic ions generated in plasmas can introduce defects into the lattice and significantly alter material properties.[51] Thus, when developing ALE techniques for thinning 2D materials, the transport properties must be measured and should have comparable transport properties to exfoliated or chemical vapor deposition (CVD)-grown material of equivalent thickness. Soft plasma etching techniques which rely on low power SF_6 and N_2 plasmas have enabled the removal of MoS_2 while mitigating energetic ion damage in the remaining layers.[52] Another way to achieve this may be via a three-step process, in which two half-reactions are used for material removal and a third reaction is used to heal defects (such as a re-chalcogenization process for TMDCs).

ATOMIC MODIFICATION

Phase patterning

Properties of 2D materials can be significantly tuned by slight atomic modifications in the form of phase engineering, defect engineering, and doping. Spatial control of these atomic modifications enable the formation of junctions within single layers of 2D materials in an edge-on manner. Phase engineering in TMDCs has garnered much attention due to several polytypes, which can be formed that possess drastically different electronic and optical properties. Metal atoms in the 2H phase have trigonal prismatic coordination with hexagonal symmetry, as shown in Fig. 2a.[53] In the 1T polytype, metal atoms are octahedrally coordinated with tetragonal symmetry. Other less common polytypes such as a distorted 1T and the 3R phase have also been observed.[54] The polytype, and hence electronic properties, depends upon the filling of the metal atom's d orbitals. With a filled d orbital the material takes on semiconducting properties, while unfilled orbitals result in metallic properties. Therefore, the phase polytype and band structure largely depends upon the chemistry of the 2D material. However, recent efforts have demonstrated that processing methods can induce a phase change without chemical modification, thereby enabling phase patterning to achieve multiple TMDC polytypes in a single layer. Figure 2b shows a STEM image of MoS_2 which has an atomically sharp junction between the 1T and 2H polytypes. In the case of MoS_2 the 2H phase is semiconducting, whereas 1T is metallic.[53] Therefore, the junction between 2H and 1T phases acts as a metal-semiconductor homojunction, which has ohmic behavior.[55]

Phase engineering has been achieved via a variety of processing techniques. One technique is alkali metal intercalation, which has been demonstrated using *n*-BuLi.[53,56–58] During this process, the alkali metal intercalates into the TMDC and donates negative charge due to its large electropositivity. The charge transfer drives a structural transition from the 2H to 1T phase. This solution processing technique is compatible with standard lithography, thus making it attractive for spatial phase patterning. Several direct-write processes, which are intrinsically resistless, have also demonstrated promise for phase engineering. Laser irradiation can induce the $2H \rightarrow 1T$ transition by thermally generating chalcogenide vacancies in $MoTe_2$,[55] which has a lower barrier for phase transition compared to sulfides and selenides. Conversely, it was demonstrated that laser irradiation can cause the reverse $1T \rightarrow 2H$ transition as well.[59] Therefore, laser irradiation is a promising route for selective area direct-write phase engineering. Phase transitions have also been demonstrated using electron irradiation.[60,61] In this process an intermediate α-phase is formed via e-beam irradiation, which subsequently leads to the formation of the 1T phase to release strain. Gaining clearer understanding of the mechanism of phase change induced by laser and electron beam irradiation should enable more controlled direct-write phase transformation and should be studied in more detail in the future. A comprehensive review of phase engineering techniques can be found elsewhere.[54]

To date, phase patterning has largely been used to lower the contact resistance of TMDC devices, by inducing the formation of the metallic 1T phase beneath metal contacts.[53,55,58] A schematic of such device is shown in Fig. 2c.[55] The contact resistance was lowered from 1.1 kΩ μm for 2H contacts to ~0.2 kΩ μm for 1T contacts using this technique.[53] Inducing an ohmic contact between 2H/1T TMDCs also can increase FET device mobility and reduce subthreshold swing while maintaining a high on/off ratio. The immense benefits of phase engineering on FET device performance warrants the inclusion of this processing technique when fabricating high-performance devices. Of the demonstrated phase engineering techniques, ion intercalation seems most promising for incorporation into device fabrication, as it is a solution-based process, which is compatible with lithography. Phase engineering also has potential for fabricating atomically thin circuitry in single flakes of TMDCs by spatially inducing the formation of metallic 1T regions. For the laser techniques to be practical, future studies need to explore whether standard ArF 193 excimer laser lithography tools can be used with lithographically defined opaque regions for selected area phase engineering.

Defect and dopant patterning

Defect engineering is another means to atomically modify 2D materials and control their physical properties. Point defects (0-D) have been thoroughly studied for many common group 6 TMDCs. Two common point defects are vacancies and interstitials. Figure 2d shows a schematic and band structure for pristine and selenium deficient $MoSe_2$ which contains Se vacancies. Defects such as chalcogen vacancies may act as a highly localized dopant, as evident by intragap states generated which are nearly dispersionless at low defect concentrations.[62] Of course, the specific properties of a defect vary significantly depending on the material composition. Line defects (1-D), also have interesting properties with implications on the electrical transport. For example, certain types of twin and tilt grain boundaries that occur in CVD-grown TMDCs can behave as 1-D metallic wires[63–65] which have been used to form gate-tunable memristors.[66] It is also predicted that the majority of edge termination states behave metallically for MoS_2,[67,68] with some behaving ferromagnetically.[69,70]

Point defects, such as transition metal vacancies and especially chalcogen vacancies, in TMDCs can occur intrinsically; however, methods have been explored to pattern defects in 2D materials, hence enabling spatially precise defect engineering. Although chalcogen vacancies can be generated in situ during synthesis,[71] the focus here is post-synthesis defect introduction as it is more suitable for selected area defect nanopatterning. Several direct-write techniques have been developed utilizing focused electron

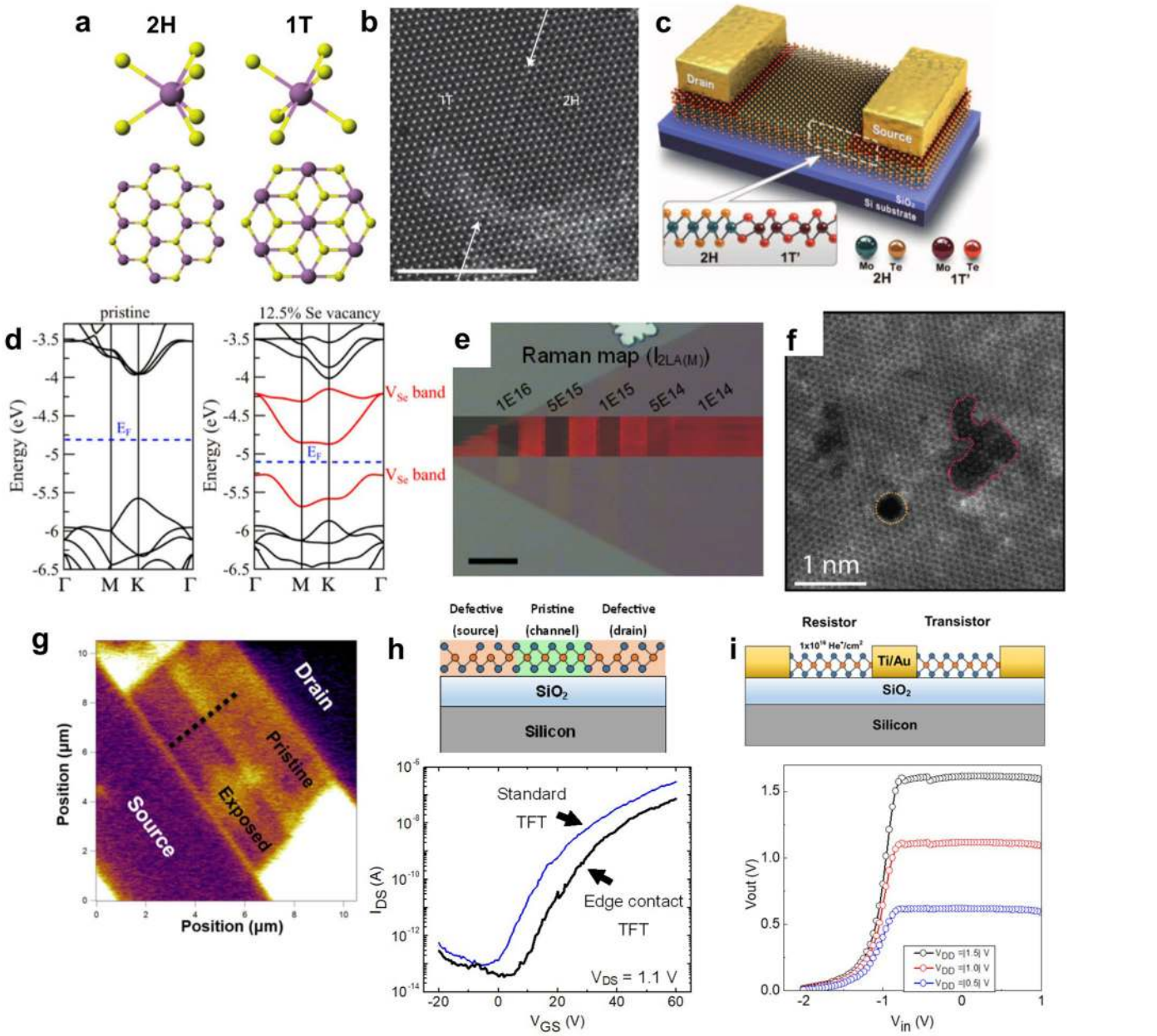

Fig. 2 Phase and defect patterning. **a** Crystal structures of the 2H and 1T phases, respectively. In the upper diagram, trigonal prismatic (left) and octahedral (right) coordinations are shown. The lower panel shows the *c*-axis view of single-layer TMDC with trigonal prismatic and octahedral coordinations. Atom color code: purple, metal; yellow, chalcogen. **b** High-resolution transmission electron microscope image of an atomically thin phase boundary (indicated by the arrows) between the 1T and 2H phases in a monolayered MoS_2 nanosheet. Scale bar, 5 nm (reprinted by permission from ref. [53] copyright Springer Nature 2014). **c** Schematic diagrams of a FET device with a 1T′/2H phase homojunction (reprinted from with permission from ref. [55] Copyright 2015, American Association for the Advancement of Science). **d** Calculated electronic band structures of single-layer $MoSe_2$ with different Se vacancy concentrations (reprinted from ref. [62]). **e** Raman map of a WS_2 flake plotting the intensity of the 2LA(M) peak. The WS_2 flake was exposed to doses varying from 1×10^{14} to 1×10^{16} He^+ cm^{-2} (inset). Scale bar is 10 μm. Raman map is overlaid on an optical micrograph (reprinted with permission from ref. [77] Copyright 2017, John Wiley & Sons). **f** Pores in MoS_2 generated by oxygen plasma and MoO_3 sublimation (reprinted from ref. [82]). **g** Kelvin Probe Force Microscopy (KPFM) image of a WSe_2 TFT in which half of the channel with exposed with a dose of 5×10^{14} He^+/cm^2 (reprinted with permission from ref. [75] Copyright 2016 Nature Springer). **h** Schematic of edge contact FET. Source and drain are fabricated from NNH WS_2 (exposed to a dose of 1×10^{16} He^+ cm^{-2}). The FET channel is pristine (unexposed) WS_2. Resultant transfer curves of edge contacted device. **i** Schematic of atomic layer inverter created by utilizing exposed and pristine material on a single flake. Input (Vin)–Output (Vout) voltage characteristics of a WSe_2 atomic layer inverter which was gated with an ionic liquid (reprinted from with permission from ref. [77] Copyright 2017, John Wiley & Sons)

and ion beams for defect engineering. Sufficient energy transferred to MoS_2 by electron irradiation has been shown to generate vacancies with a high degree of precision which can agglomerate into line defects.[72,73] More recently, focused helium ions have been used to pattern defects in MoS_2,[74] WSe_2,[75–77] WS_2,[77] and $MoSe_2$.[62] The much higher mass He^+ (compared to e^-) can be used to introduce vacancies which can agglomerate into pores with a greater yield. It is worth noting that ion irradiation transfers sufficient energy to both metal and chalcogen atoms to generate vacancies but energetics favor the formation of chalcogen

vacancies due to their lower mass.[78] Figure 2e shows an optical image and an overlaid Raman map of the E^2_g mode, which demonstrates the spatial control of defects introduced within a single flake of material using He^+ irradiation.[75] Vacancy introduction using focused electron and ion beams has the benefit of extremely high resolution. They also enable a high degree of control over the vacancy concentration by tuning the exposure dose. These factors are ideal for the rapid discovery of emergent properties introduced by defects of varying concentration. Notably, recent work has demonstrated atomic resolution for vacancy introduction and manipulation in graphene using a STEM.[79] This technique will be further discussed in the direct-write patterning section, as it can have important implications on the processing of other 2D materials. However, processes compatible with standard lithography need to be developed for large area defect nanopatterning. A logical extension of the direct-write focused electron and ion beam techniques is plasma processing with plasma species that do not react to form compounds with the 2D material. For example, an Ar plasma has been used to generate atomic scale vacancies in MoS_2 and WS_2.[80] A hydrogen plasma has also been shown to introduce defects into TMDCs, which may hinder its use for certain processing techniques, such as top-gate dielectric deposition, during devices fabrication.[51] It was demonstrated that remote hydrogen plasma can be used to completely strip the top layer of chalcogen atoms, thus enabling the formation of Janus monolayers of MoSSe.[81] Other plasma exposures such as oxygen and fluorine plasmas have also shown potential to generate defects 2D materials, although some degree of doping may occur. For additional information refer to the etching portion of this review. It is worth noting that some oxide passivated layers have high vapor pressures. An oxygen plasma exposure followed by high vacuum sublimation of the oxide can be used to form pores within MoS_2, as shown in Fig. 2f.[82] This property has led to oxidation and subsequent sublimation to be used as an ALE technique.[44]

Nanopatterning of defects in TMDCs have introduced additional functionality in 2D materials, leading to new optical and electronic devices. Chalcogen vacancies can induce sub-bandgap emission peaks and increase the overall photoluminescence intensity in TMDCs.[83] Optical properties of other intentionally doped defective material have been further studied in several other publications.[84,85] Defect introduction, such as vacancy generation, can also be used to tune the local Fermi energy in TMDCs. Figure 2g shows Kelvin Probe Force Microscopy (KPFM) on a WSe_2 device in which chalcogen vacancies were introduced into half of the channel and thus formed a p–n homojunction with a demonstrated photovoltage.[75] The creation of such homojunctions by defect patterning 2D enables the formation 2D diodes and can serve to pattern p–n junctions within a single flake of material. It was demonstrated that an extensive vacancy concentration can induce metallic transport in TMDCs,[74] and post-synthesis creation of excessive mirror twin boundaries can do the same.[65] Recent work has shown that at high enough defect concentrations, percolating networks of pores and edge states form within TMDCs which first-principles simulations reveal to be the origin of metallic transport,[77] although oxidation of edge states may also contribute.[86] Therefore, patterning conductive regions that are insensitive to gate modulation via defect engineering has been utilized to direct-write atomically thin circuitry onto single flakes of WSe_2 and WS_2. Figure 2h shows a schematic and transfer curves for an edge-contacted transistor in which percolating networks of agglomerated vacancies were patterned and utilized to create a high conductivity source and drain. Defect patterning was also utilized to create a logic gate out of a single flake of WSe_2 and WS_2. Figure 2i shows a schematic of an inverter, in which metallic conduction from defect engineering was utilized to write the load resistor in series with pristine WSe_2 on the same flake, which serves as a transistor. Input–output curves for this resistor-loaded inverter is shown in Fig. 2i and a gain of >5 indicates that the defect engineered inverter is suitable to circuitry applications. Defect engineering in 2D materials, MXenes in particular, also has immense potential for creating materials ideal energy storage applications. For electrode applications, point defects and pores enable pathways for electrolyte solutions to intercalate into the material more rapidly.[87] Certain defects can also act as active sites for redox reactions. Hence, defect patterning could be a promising technique for patterning electrodes for supercapacitor or other energy storage devices.

Doping of 2D materials can also be used as an atomic modification tool for tuning the optical, electronic, and structural properties and often arises from defect introduction. In general, the techniques reported include in situ substitutional doping[88,89] as well as ex situ doping. Here we will focus on ex situ doping, as it enables nanopatterning of defects within the lattice. In order for dopants to be nanopatterned into 2D materials for spatial control of properties, doping techniques should either be direct-write in nature, or compatible with standard lithography. To date, the most studied technique to spatially introduce defects is plasma treatment with species that form non-volatile compounds with the 2D material. Oxygen plasma has been used to generate chalcogen vacancies and form transition metal oxides in order to tune the bandgap of MoS_2.[90] However, oxygen plasmas rapidly attack many carbon-based resist layers, thus care must be taken to use appropriately thick resist layer or use a sacrificial hard mask layer if dopants are to be patterned. Furthermore, many plasma species which are more friendly (have higher selectivity) with standard lithography have been used to dope 2D materials, such as N_2,[91] SF_6,[92] and H_2[93] doping to name a few. Some other doping techniques which are compatible with lithography include functionalization with metallic nanoparticles,[94] as materials such as Au can induce p-type characteristics in MoS_2 by charge transfer,[95] and a plethora of molecular and chemical doping techniques.[96–98] Recent work demonstrated that by intercalation of Cu and Co into SnS_2 parent material, electronic properties can be greatly tuned, and seamless atomic p–n metal junctions were obtained.[99] The powerful technique of intercalation doping could be applied to many 2D materials since the relatively large van der Waals gap facilitates intercalation of atoms. The development of doping and alloying techniques will provide a near-infinite combination of dopants and 2D materials, which has, by analogy, been critical to the band gap engineering and abrupt junction doping achieved in standard semiconductors historically.

EMERGING NANOPATTERING AND LITHOGRAPHIC TECHNIQUES

Lateral heterostructures

Atomically thin circuitry can be created by stitching together 2D materials with varying composition and properties to create lateral heterostructures. This can enable the formation of metal–semiconductor junctions, p–n junctions, and other semiconductor–semiconductor junctions, which are critical for integrated circuitry. The formation of lateral heterostructures can provide a critical breakthrough toward the realization of flexible and transparent circuits, which are becoming more prevalent with the rise of the Internet of Things. To date, several strategies have been explored to create 2D lateral heterojunctions, namely: (1) non-epitaxial growth, (2) epitaxial growth, and (3) selectively converting regions of a 2D material into another material. The aim of this section is to highlight these emerging techniques and comment on the compatibility with nanopatterning techniques toward the intelligent design of heterostructure geometries.

Non-epitaxial formation of 2D lateral heterojunctions have perhaps demonstrated the most promise for creating single layer circuitry. Zhao et al.[100] and Ling et al.[32] created non-epitaxial

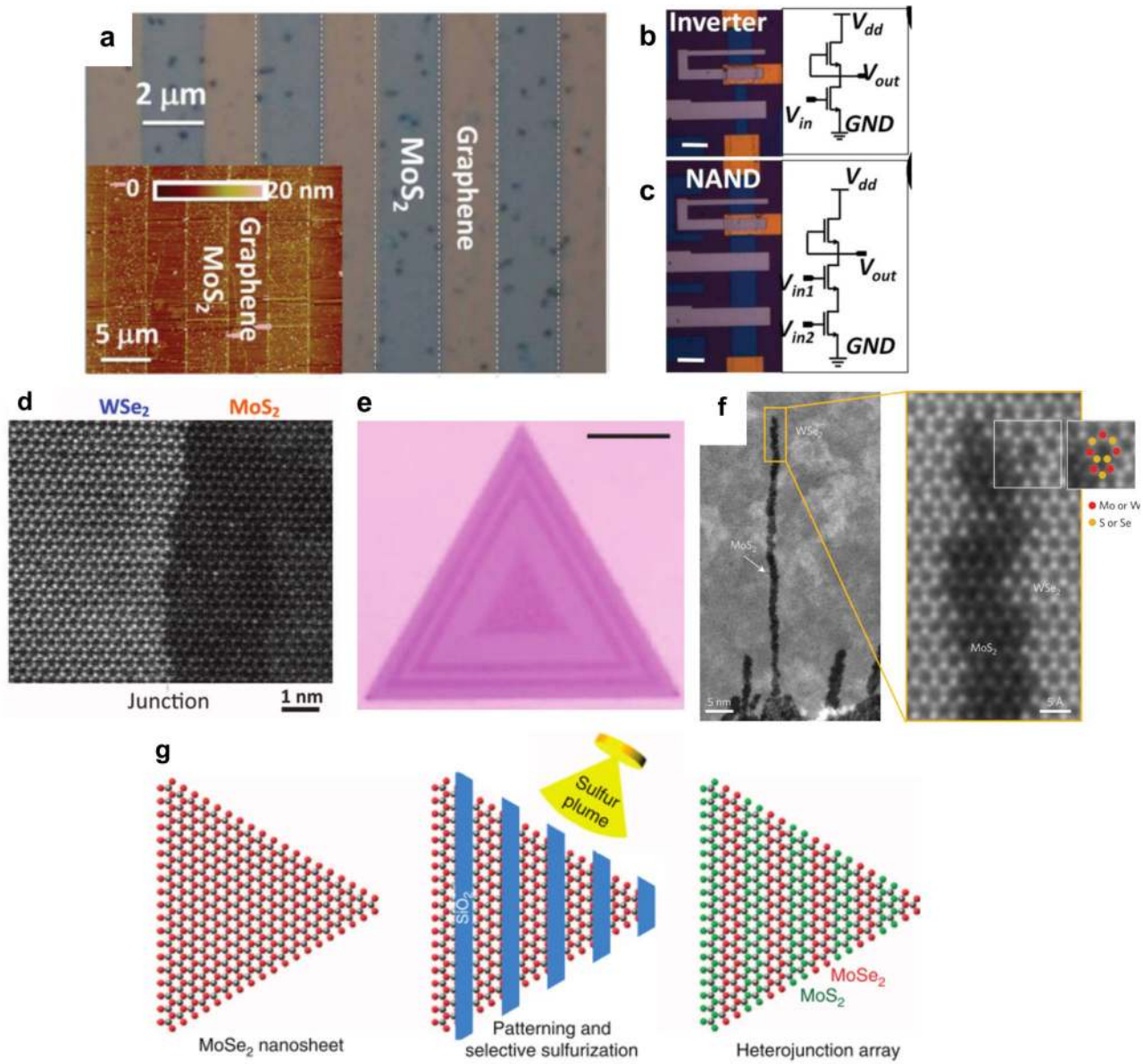

Fig. 3 Lateral heterostructures. **a** Typical optical images of the graphene–MoS_2 periodic array. Microscopy images and transistor-level schematics of the **b**, the inverter **c**, and the NAND gate (reprinted with permission from ref. [32] Copyright 2016 John Wiley & Sons). **d** High-resolution STEM images taken from the WSe_2–MoS_2 in-plane heterostructure (reprinted with permission from ref. [103] copyright 2015 American Association for the Advancement of Science). **e** Optical image in which the WSe_2 and $MoSe_2$ heterostructure can be distinguished by their optical contrast. Scalebar is 10 μm (reprinted with permission from ref. [104] copyright Springer Nature 2018). **f** ADF-STEM image of MoS_2 1D channels embedded within WSe_2. The channel ends with the 5|7 dislocation. The same section is shown to the right with the atoms labeled (reprinted by permission from ref. [114] copyright 2018 Springer Nature). **g** Schematic illustration of the experimental steps for the formation of $MoSe_2$/MoS_2 heterojunction arrays by selective conversion (reprinted from ref. [116])

heterostructures by first lithographically patterning and etching graphene. Dangling carbon bonds and resist residue subsequently served as nucleation sites for the CVD growth of MoS_2 in the regions where graphene was etched. Lattice mismatch results in nanoscale overlap of the two materials at the junction. The graphene/MoS_2 heterojunctions (Fig. 3a) acts as a metal/semiconductor junction with low contact resistance compared with traditional metal contacted devices. From this technique atomically thin inverters (Fig. 3b), logic gates (Fig. 3c), and edge contacted transistors were synthesized, demonstrating potential to create atomically thin flexible circuitry. Non-epitaxial growth of 2D lateral heterostructures should be compatible with a large number of 2D materials, including most graphene/TMDC combinations.[101] Because this technique is compatible with lithography, a large number of device architectures can be fabricated with relative ease.

Epitaxial growth is convenient for the formation of atomically sharp lateral heterojunctions without alloying at the interface. In 2014, Liu et al. achieved the epitaxial growth of hexagonal boron nitride/graphene to create lateral heterostructures.[102] Later, the formation of WSe_2–MoS_2 lateral p–n junctions were also demonstrated.[103] A STEM image of the atomically sharp junction is shown in Fig. 3d. This heterojunction is created by first growing WSe_2 via van der Waals epitaxy followed by edge epitaxy of MoS_2. This type of two-step growth process enables the formation of heterojunctions between TMDCs of different metal and chalcogen species. Therefore, p–n junctions were formed which exhibit a photovoltaic effect. Recently, one-pot growth was developed for

creating 2D lateral heterojunctions.[104] This synthesis technique uses a single heterogeneous solid source, and heterojunctions are created by changing the composition of the reactive gas. The presence of water vapor during growth allows selective control of precursor oxidation and volatilization, enabling the formation of distinct TMDCs. Figure 3e shows an example of $MoSe_2/WSe_2$ structures which were created in this manner. Other works have demonstrated the formation of various TMDC lateral heterojunctions by sequential CVD processes.[105–113] However, the lateral heterostructure formation generally results in the formation of concentric junctions dictated in shape by the geometry of the flake. This is not as useful as the aforementioned processes for the patterning of single layer circuitry. A logical follow on to this work is lithographically patterning and etching practical device geometries and developing masking layers in which selected area lateral epitaxial growth of only certain edges are promoted. If this can be accomplished, it should enable epitaxial growth in patterns dictated by lithography, not the flake's growth geometry.

Recently, a dislocation catalyzed approach has been developed to epitaxially grow sub-nanometer channels of MoS_2 in WSe_2 (Fig. 3f).[114] In this process, lattice mismatch at lateral interfaces introduces misfit dislocations where the core of the dislocation exhibits high reactivity to growth precursors. This enables small heterostructure channels to form behind an advancing dislocation core in the presence of a growth precursor. These sub-nanometer channels exhibit type-II band alignment which could be promising for charge separation. With control over dislocation spacing, periodic nanochannels could be formed as a 2d analog to a multilayer superlattice. Van der Waals materials have shown exceptional promise for photovoltaic applications,[115] and the formation of such superlattices could enable the formation of high quantum-efficiency photovoltaic devices and light emitting devices, among other electronic applications. With advancements in defect engineering, misfit dislocations could be engineered which should enable the formation of superlattices to be realized.

The patterning of 2D lateral epitaxial heterojunctions by selectively converting $MoSe_2$ to MoS_2 provides an alternative, ex situ technique for heterojunction synthesis.[116] This has been done by patterning a masking layer over an $MoSe_2$ flake using electron beam lithography, and then exposing the patterned $MoSe_2$ to a sulfur pulsed laser plume. The sulfur content was tunable in the areas exposed to the sulfur plume and thus MoS_xSe_{1-x} alloying was possible. A schematic of the conversion process is shown in Fig. 3g. For conversion processes, it is worth noting that most are irreversible in nature. For example, $MoSe_2$ can be converted to MoS_2 because the sulfurization of molybdenum occurs at a lower temperature than the selenization. Therefore, the reverse process is not energetically favorable without deteriorating the remaining film. The conversion process is also most useful for creating heterostructures with different chalcogen species, as post-synthesis metal replacement is not straightforward. The selective conversion process provides exceptional promise for the creation of lateral heterostructures and chalcogen alloying toward the formation of single layer circuitry because of its compatibility with standard lithographic techniques. Additionally, MoS_2 has been masked with a sacrificial resist layer and treated with oxygen plasma to create lateral heterojunctions.[117] Specifically, this creates a MoO_3/MoS_2 junction which exhibits rectifying behavior and demonstrates the promise of simple plasma treatments for the nanofabrication of atomically thin lateral heterostructures.

Direct-write patterning

Direct-write patterning of 2D materials can enable high-resolution processing in a highly controlled manner. However, most direct-write techniques have prohibitively low-throughput for industrial applications. Therefore, direct-write processes are largely limited for rapid prototyping and studying emerging material properties and device structures. Direct-write nanoscale processes typically require the utilization of a high-resolution probe. In general, the probe can be (1) a focused particle beam, (2) a focused photon beam, or (3) a physical probe tip.

Focused particle beams, such as electron or ion beams, have been used for a plethora of direct-write processing techniques. When patterning with focused particle beams, ion–solid interactions must be considered to discern the potential of the particle beam for the given application. The energy transferred from the charge particle to the target material (via electronic or nuclear interactions) determines its applicability and depends on variables such as particle mass, target material mass, and beam energy, among others. Detailed ion–solid interaction studies and simulations of 2D materials have been performed (for details, see ref. [78]). For example, electron beams have demonstrated potential to induce phase changes in TMDCs; however, the low mass of electrons (and low nuclear stopping power) limit its use in direct-write nanopatterning of 2D materials by milling/sputtering. One exception is some recent work in which individual defects are manipulated with a STEM.[79,118–121] This technique demonstrated controlled introduction and motion of substitutional Si defects in graphene.[79] Figure 4a shows two Si atoms in a graphene lattice which were assembled into a diatomic cluster. Atomic motion is achieved by scanning a sub-scan area adjacent to the Si atoms. Irradiation with the electron beam transfers sufficient energy to the lattice to overcome the energy barrier for interstitial movement. Similar atomic manipulation should be achievable with a plethora of 2D materials. For example, transmission electron microscopes have been used to sculpt nanoribbons in materials such as BP[122] and TMDCs.[123] Manipulating materials on the length scale of single atoms in a direct-write manner can be used to study the quantum nature of individual defects and interstitials. Implications of such control will be discussed in future outlooks.

Beyond single atom manipulation in 2D materials, gas-assisted processes have been developed for electron beam direct-write. Electron beam-induced etching (EBIE) has been conducted by flowing a XeF_2 precursor gas in an SEM while exposing MoS_2 with the electron beam.[124] The electron beam inelastically dissociates the XeF_2 into Xe and F radicals, where the F radicals react with the MoS_2 to form volatile compounds thus etching the material in a direct-write manner.

Heavier ions can be used to pattern 2D materials via a similar gas-assisted process or by simple sputtering.[125,126] Several promising demonstrations have shown that the sub-nanometer focused He^+ beam can be used to mill nanoscale structures into 2D films.[74,127,128] This should enable the study of quantum confinement in various 2D materials; however, the sputter yield is very low due to its relatively low mass and backscattered and recoil atoms can cause unintended damage in areas surrounding to the patterned region.[129,130] Therefore, gas-assisted processes are a promising approach to increase the efficiency of material removal and thus minimize peripheral damage. Focused helium ion beam-induced etching (IBIE) with XeF_2 precursor gas has been used to directly etch sub-10 nm nanoribbons in WSe_2.[76] Analogous to the EBIE process, the ion irradiation drives dissociation of the XeF_2 precursor gas, and both chemical and physical mechanisms contribute synergistically to etch the WSe_2 film. A schematic of this process is shown in Fig. 4b. The IBIE etching process enables the formation of high-quality nanoribbons which demonstrate Raman anisotropy. Similar phenomena have been observed in MoS_2 nanoribbons formed by He^+ milling.[127] An image of the sub-10 nm aligned array of nanoribbons obtained from this process is shown in Fig. 4c. Such techniques should enable the experimental study of nanoscale geometries such as TMDC nanoribbons which have largely been confined to simulation studies.[131,132]

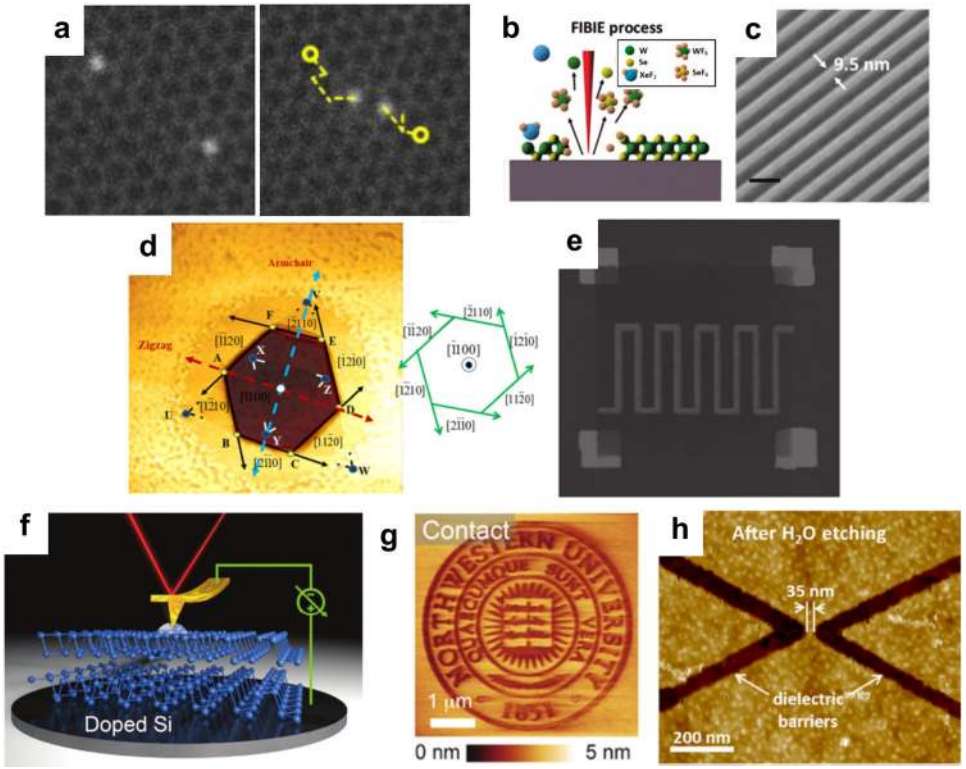

Fig. 4 Direct-write patterning. **a** STEM image of creation of a Si dimer within a graphene lattice via e-beam manipulation (reprinted from ref. [79]). **b** Schematic of focused ion beam-induced etching of WSe_2. **c** SEM image of WSe_2 nanoribbons created with the FIBIE process. The scale bar represents 40 nm (reprinted with permission from ref. [76] Copyright 2017, John Wiley & Sons). **d** The 3-D interpretation of an AFM image of a single laser-induced hexagonal void. The crystallographic orientation of the plane of the MoS_2 flake is depicted from the orientation of the hexagonal void (reprinted with permission from ref. [133] copyright 2017 AIP Publishing). **e** A typical photograph of the as-prepared MoS_2 film micro-supercapacitor. Each of the finger electrodes is 4.5 mm long, 820 μm wide, and the spacing between two finger electrodes is 200 μm (reprinted with permission from ref. [136] Copyright 2013 John Wiley & Sons). **f** Schematic illustration of the DC CAFM patterning of BP crystals setup. **g** Contact mode AFM image of the Northwestern University logo patterned by CAFM (reprinted with permission from ref. [142] Copyright 2017 John Wiley & Sons). **h** Pattern etched into WSe_2 by scanning probe-induced oxidation and subsequent H_2O etching (reprinted from ref. [143])

Photon beams have also been used as a probe for direct-write processing in 2D materials. Focused lasers have been used to etch MoS_2 and WS_2 in a controllable manner with the likely mechanism being thermal sublimation or oxidation/evaporation in ambient conditions.[133–135] This technique can be used to etch features such as nanoribbons into MoS_2.[133] Voids formed from the etching process also exhibited hexagonal geometry, thus revealing the orientation of the lattice (Fig. 4d). Devices such as supercapacitors have also been demonstrated by cutting interdigitated geometries into continuous printable MoS_2 films,[136] joining laser-induced graphene as a promising direct-write supercapacitor made from 2D materials.[137,138] See Fig. 4e for an image of a direct-written MoS_2 supercapacitor. Some other demonstrated laser-induced processing techniques for 2D materials include laser oxidation of black phosphorous[139] and laser thinning of MoS_2.[140] It is worth noting that laser-induced processes generally lack the resolution of focused particle beams (such as ions). For instance, diffraction limits the fundamental probe size for far-field lasers. Additionally, heat transport can result in a heat affected zone surrounding the directly irradiated material, thus further limiting resolution. Therefore, laser processing techniques are best suited for applications where relatively large area processing is desired. Advancements in laser processing techniques with industrial laser cutters and laser engravers should enable roll-to-roll processing with high throughput.

Physical probe tips offer another means for direct-write processing of 2D materials. In 1992, Delawski et al. demonstrated that an atomic force microscope (AFM) could be used to etch individual layers of $SnSe_2$ in a controllable manner.[141] Since this study, scanning probe etching has been used for more sophisticated patterning of 2D materials, including the use of a conductive AFM to etch black phosphorous.[142] In this technique, direct current is applied to the BP which causes local anodic oxidation. A schematic of this techniques is shown in Fig. 4f. The residual phosphorous oxoacids can be rinsed from the surface leaving behind the thinned BP. This enables high-resolution direct-write thinning as demonstrated in the AFM image in Fig. 4g. Similar scanning probe-induced oxidation has been used to pattern TMDCs, specifically WSe_2. The oxidized WSe_2 was then etched by immersion in water. Therefore, sub-40 nm structures can be direct written (Fig. 4h) by probe-induced oxidation and subsequent etching.[143] Scanning probe-induced patterning can offer high patterning resolution given the atomic resolution of some scanning probe techniques. Throughput, however, is expected to be limited, thus making scanning probe patterning of 2D materials most useful for fundamental studies and rapid prototyping.

Novel lithographic techniques

Some emerging lithographic techniques have been developed to pattern and process complex geometries of 2D materials for novel applications. These techniques do not rely on standard planar lithography that is typically carried out with the use of a resist layer. One example includes the stamping of flexible micro-supercapacitors from MXene ink.[144] Specifically, 2D $Ti_3C_2T_x$ device

structures were stamped onto paper substrates. Stamping of devices made of 2D material inks should enable high-throughput low-cost creation of electronic devices, which is attractive for industrial applications.

Recently, several groups have demonstrated patterning of 2D materials by synthesis on pre-patterned substrates. Micromolding techniques have been applied to fabricate nanoribbons from a thiosalt $(NH_4)_2MoS_4$ solution.[145] The widths of the nanoribbons were as narrow as 157 nm. An alternative method for patterning anisotropic structures includes depositing on rippled substrates. MoS_2 films which were deposited on a rippled SiO_2 substrate were shown to exhibit Raman anisotropy.[146] Patterning on pre-patterned substrates can enable the study of emerging materials properties associated with strain and shape anisotropy[147]; however, fabricating electrical or optoelectronic devices from such methods may prove difficult. A lithographic technique to create free-standing metal (e.g., Mo, W, Sn) structures was demonstrated, which can then be sulfurized via a CVD process.[148] This can be used to synthesize three-dimensional free-standing TMDC structures and is compatible with standard lithography, which resulted in the fabrication of high-performance gas sensors. Similar techniques could be useful whenever it is desirable for TMDCs to have a high aspect ratio to the surrounding medium, such as for catalytic and energy storage applications.

There have also been recent advances in using self-assembled masks to pattern various 2D materials. With controlled self-assembly, programmable complex structures can be patterned as well as structures which would exceed the resolution limits of standard lithography. One such method is to pattern with block copolymers (BCP). BCP lithography with an oxygen plasma etch has been used to pattern MoS_2 with features down to 4 nm.[41] This technique can yield arrays of nanodots, nanorods, and nanomeshes. In fact, BCP patterning has been used to fabricate sub-10 nm MoS_2 field-effect transistor channels (which will be further highlighted in the emerging devices section).[149] Other techniques, such as the self-assembly of DNA nanotubes,[150] have also demonstrated promise for complex patterning of 2D materials. Significant advances in the self-assembly of masking layers and other emerging lithographic techniques could enable patterning which does not experience the limitations of standard optical and e-beam lithography. These emerging techniques should continue to be developed to expand the nanopatterning capabilities of a diverse range of 2D materials.

NEW PHYSICAL PHENOMENA AND DEVICES

Thus far in this article, a detailed description of various methods for spatially controlled modification and synthesis of post-graphene 2D materials has been presented. A variety of structures have been patterned using these methods at various length scales. However, the important and relevant length scales are those of the wavelength of interacting photons and mean-free path of electrons in these materials. For the case of graphene, which is a semi-metal, lateral patterning-induced confinement even at the μm scale results in confinement of collective charge oscillations upon illumination in the terahertz regime,[151] this is manifested in strong surface plasmon polariton (SPP) absorption in the mid-infrared part of the spectrum in <100 nm wide graphene nanoribbons.[152] Similar plasmonic resonances have been predicted and computationally simulated for BP.[153,154] However, the presence of a band gap and consequently lower carrier density compared to the semi-metallic graphene means that the SPP resonances only occur in far IR spectral range even for ribbon width of ~100 nm. A unique feature of the BP plasmonic ribbons is asymmetry introduced in the plasmonic resonance owing to the asymmetry in the crystal structure and consequently the optical dielectric function.[153,154] The patterning techniques discussed in the above sections are sufficient to pattern BP in <100 nm dimensions. This combined with electrostatic gate-tuning[155] should allow for observation of tunable plasmons; however, no experimental evidence is yet available for SPPs in BP nanoribbons. Possible challenges could be lack of sufficient oscillator strength or sufficient carrier density in the BP, which prevents plasmon observation within the typical infrared detector range (~50 μms).

While the optical dielectric function has been shown to modulate with electric field, another interesting route to modulation of band-structure and consequently the optical-dielectric function is via localized, high-magnitude strain. Such strain can either be introduced via lithographic patterns on the substrate or via rippling of elastomeric substrates, as seen in Fig. 5a.[156] Periodic compressive and tensile strain modulation can decrease or increase the band gap, respectively, as compared to the unstrained state, evidenced from the change in band-edge absorption (Fig. 5b).[156] Strain-induced changes in band structure can serve as an important tool in introducing quantum confinement.[157] In particular, tensile strain is known to shrink the band-gap in TMDCs. This strategy can be effectively used to create strain gradients in 2D TMDCs (WS_2 in this case) draping over tall posts etched in Si/SiO_2. The band structure changes induced in WS_2 at the top of the post as a result of the strain forms a localized quantum-dot (QD) feature in the electronic structure (Fig. 5c). This results in enhanced photoluminescence emission from the QD (Fig. 5d) in addition to sharpening of the spectral line suggesting quantum emission of single photons.[158] A similar strain-induced phenomena has been observed in strained WSe_2,[159] suggesting it is applicable for many TMDCs. The electronic band-structure in TMDCs can also be locally modulated to create a QD via purely electrostatic doping-induced confinement.[160,161] If electrostatic gates are designed to confine electrons and charged excitations in small regions (Fig. 5e), then the emission from the resulting confined region can be electrostatically controlled to go from predominantly neutral excitonic (χ) to confined, negatively charged excitonic (χ^-) emission in a monolayer of $MoSe_2$[161] (Fig. 5f).

Advances in nanoscale patterning and extreme miniaturization has also led to lab scale demonstrations of electronic transport phenomena in the same example of electrostatically confined QD discussed above. In this case, single electron tunneling and coulomb blockade is observed in a tri-layer $MoSe_2$.[161] QDs from TMDC monolayers have also been directly fabricated using e-beam lithography; however, not noticeable sharpening or enhancement in emission has been observed likely due to increased non-radiative recombination from the edges.[162] However, the confinement potentials with advanced nanofabrication are not limited to 0D quantum dots. Field-effect devices with channel lengths <mean-free path have also been demonstrated in 2D semiconductors. Indeed, 2D materials are ideal candidates for downsized transistors since they are largely unaffected by short-channel effects (SCEs).). To evaluate the prevalence of SCEs for a certain material and device geometry, the screening length is determined, $\lambda_{2D} = [(\varepsilon_{2D}/\varepsilon_{ox})t_{TMD}t_{ox}]^{1/2}$, where ε_{2D} is the dielectric constant of the 2D material, ε_{ox} is the dielectric constant of the gate oxide, and t are the respective thicknesses. To prevent SCEs, a small screening length is necessary to prevent punch through as well as subthreshold current from drain-induced barrier lowering. Owing to its atomic thickness and generally low dielectric constants, 2D materials typically have small screening lengths which enables the formation of high-performance, sub-10 nm transistors. Recent advancements in nanofabrication techniques have enabled the fabrication of demonstration of high-performance, short-channel FETs. These devices have been fabricated by standard e-beam lithography; however, novel techniques have been developed to create sub-10 nm channel lengths. Corrosion cracks along a Bi_2O_3 cleavage plane were used to define a sub-10 nm in MoS_2.[163] Directional deposition has also been utilized to

define a 20 nm channel for the fabrication of short-channel BP FETs.[164] If short-channel devices can be demonstrated by the formation of 2D heterojunctions, this should provide a building block toward the ultimate realization of high-performance stackable electronics. Palacios et al. have demonstrated that via block co-polymer patterning and phase engineering, edge-contacted short-channel MoS_2 devices can be realized by using the 1T′ phase as source and drain electrodes.[149] For 2D materials to offer a viable replacement to the state-of-the-art Si-based technology, further downscaling and optimization of 2D devices should be pursued.

FUTURE OUTLOOKS

The first demonstration of a semiconductor switch was that of the point contact transistor using germanium single crystals in 1947 by Bardeen, Shockley, and Brattain. Since then it took roughly 16 years to arrive at the standard MOSFET circuit design that is prevalent in today's ICs. In comparison, the first high-performance transistors from MoS2 were demonstrated in 2011, while the first report on lab-scale microprocessors and wafer scale high-quality material appeared in 2016–2017. Despite revolutionary advances in microfabrication and semiconductor processing technology, a time scale of 5–6 years from first basic device demonstration to microprocessors is a breathtaking pace of progress. Nonetheless, modern semiconductor electronics and optoelectronics is at a very advanced level of miniaturization, complexity, and performance, therefore necessitating stringent performance targets for devices of any emerging materials. As a result, much more progress is desired in terms of controlled spatial and structural modulation of the emerging 2D materials discussed in this review.

A prominent dilemma with any material vying to replace silicon is the inertia of a trillion $ industry dedicated and developed around silicon. Therefore, unless the new candidate offers orders of magnitude performance enhancements or unprecedented advantage in fundamental design of electronics and opto-electronics technology, it is unlikely to attract enough attention or capital for efforts that challenge silicon. Therefore, in the near term, the focus with regard to 2D semiconductors must be on the basic science of materials development, nanofabrication, and understanding of device physics. In the medium term, the emphasis must lay on identifying key properties, areas, and

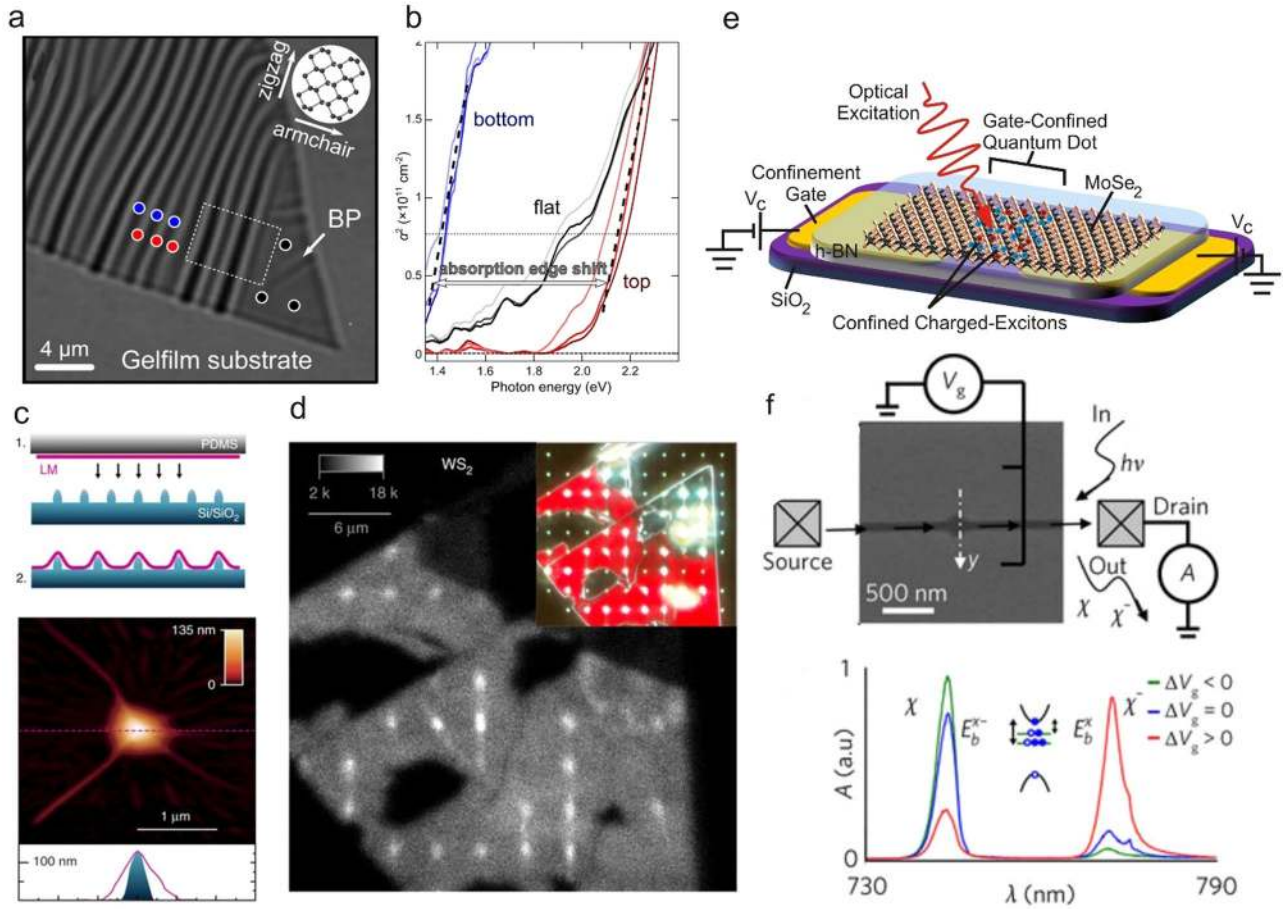

Fig. 5 New physical phenomena and devices. **a** Optical micrograph of a rippled/periodically strained flake of black phosphorus (BP) on a gel-film substrate. **b** Optical absorption spectra color coded with spots in a showing shift in absorption band edge, indicating locally strain-induced expansion/reduction of the electronic band gap (reprinted with permission from ref. [156] Copyright 2016 American Chemical Society). **c** (Top) Schematic cross section of pillar posts etched in Si/SiO_2 substrate and transfer of monolayer WS_2 using PDMS stamps. (Bottom) AFM topography and line cut of the transferred WS_2 monolayer on the pillar post. **d** Spatial map of integrated photoluminescence emission intensity over a selected region of the transferred WS_2 flake sample over posts. The WS_2 flake regions draped over posts show enhanced luminescence compared to other areas suggesting localized high-emission intensity due to reduction in band-gap and exciton funneling from nearby region of the flake. Inset shows a dark-field optical micrograph under reflection mode for the corresponding region of the sample (reprinted from ref. [158]). **e** Schematic of electrostatic gate-confined TMDC device for confining charged excitons (reprinted with permission from ref. [160] copyright Springer Nature 2018). **f** (Top) SEM micrograph of a representative device shown in e along with measurement schematic. (Bottom) Emission spectra from the confined quantum dot region as a function of V_c in **e** (equivalent to ΔV_g in **f**) showing tunable emission of neutral (χ) vs. charged excitons (χ^-) (reprinted with permission from ref. [161] copyright Springer Nature 2018)

applications, where 2D semiconductors present a distinct advantage over silicon and all other available options. Toward that end, the atomically thin nature with uniform thin-film physical form, combined with semi-transparency of monolayers to electric fields is a key point of distinction. This feature allows superior gate-tunability to heterostructures comprising 2D semiconductors enabling new classes of devices including tunneling FETs that promise low power consumption in the future. Another application where 2D semiconductors promise to stand out over the competition is unconventional format electronics where the mechanical flexibility, bendability, stretchability, and ease of integration with non-traditional electronic materials such as polymers, elastomers, and bio-materials is critical. TMDCs in particular have superior mobility, mechanical, thermal, and chemical stability over other conventional semiconductors such as organics, amorphous oxides, and carbon nanotube mats.[19]

The optical and photonic properties, however, distinguish 2D semiconductors from other materials. Not only do 2D semiconductors have some of the highest absorption coefficients observed in known materials,[115] their strong exciton binding energy (~1 eV of monolayer TMDCs) gives them the best attributes of both inorganic III-V semiconductors as well as organic materials. The ability to physically treat, process, and pattern them as inorganic quantum wells while retaining the strong excitonic properties of organics and QDs places TMDCs in a unique position of advantage in terms of integration and design conceptualization of new devices. In particular, nanofabrication and patterning can play a key role in the rational design of quantum-confined structures that allow control and manipulation of excitons for low power logic, non-chip communication, as a well form the basis of quantum devices. With that said, very little has been achieved in controlled electronic or optical confinement in post-graphene 2D materials for exploiting their optical and electronic properties. While techniques such as He^+ ion beam, electron beam, and scanning probe lithography offer hope, the end result must preserve the crystalline quality of the material and minimize collateral damage or induce charges and defects that may disrupt the transport properties or results in predominantly non-radiative recombination.[162] A promising direction to avoid such deleterious side effects would be the use of encapsulating barrier layers or develop strategies for inducing strong quantum electronic or photonic confinement without creating step edges or defects. Toward that end, in-plane growth of quantum-confined features will be an important direction moving forward.[165] Likewise, controlled growth and diffusion to create atomically sharp out-of-plane heterostructures is another unexplored area.

Overall, the science of post-graphene 2D materials is still in its infancy. However, the high rate of progress in a short time span justifies the sustained enthusiasm and excitement in research both at fundamental and applied levels. Moving forward, nanoscale patterning, defect engineering, and confinement strategies will play a key role in discovery of new properties/phenomena as well as opening up of new applications. By focusing on properties of post-graphene 2D materials that are unique and provide a distinct advantage in applications, the community stands the best chance at moving the materials and the technology up the value chain in the shortest time frame.

ACKNOWLEDGEMENTS

M.G.S. and P.D.R. acknowledge support by US Department of Energy (DOE) under Grant No. DOE DE-SC0002136. P.D.R. also acknowledges support from Center for Nanophase Materials Sciences, which is a DOE Office of Science User Facility. D.J. acknowledges support from Penn Engineering start-up funds.

AUTHOR CONTRIBUTIONS

All authors contributed to the preparation and revisions of the manuscript.

ADDITIONAL INFORMATION

Supplementary information accompanies the paper on the *npj 2D Materials and Applications* website (https://doi.org/10.1038/s41699-018-0065-3).

Competing interests: The authors declare no competing interests.

Publisher's note: Springer Nature remains neutral with regard to jurisdictional claims in published maps and institutional affiliations.

REFERENCES

1. Fiori, G. et al. Electronics based on two-dimensional materials. *Nat. Nanotechnol.* **9**, 768 (2014).
2. Packan, P. A. Pushing the limits. *Science* **285**, 2079–2081 (1999).
3. Singh, T. B. & Sariciftci, N. S. Progress in plastic electronics devices. *Annu. Rev. Mater. Res.* **36**, 199–230 (2006).
4. Kelley, T. W. et al. Recent progress in organic electronics: materials, devices, and processes. *Chem. Mater.* **16**, 4413–4422 (2004).
5. Jariwala, D., Sangwan, V. K., Lauhon, L. J., Marks, T. J. & Hersam, M. C. Carbon nanomaterials for electronics, optoelectronics, photovoltaics, and sensing. *Chem. Soc. Rev.* **42**, 2824–2860 (2013).
6. Avouris, P., Appenzeller, J., Martel, R. & Wind, S. J. Carbon nanotube electronics. *Proc. IEEE* **91**, 1772–1784 (2003).
7. Cao, Q. & Rogers, J. A. Ultrathin films of single-walled carbon nanotubes for electronics and sensors: a review of fundamental and applied aspects. *Adv. Mater.* **21**, 29–53 (2009).
8. Li, Y., Qian, F., Xiang, J. & Lieber, C. M. Nanowire electronic and optoelectronic devices. *Mater. Today* **9**, 18–27 (2006).
9. Lu, W. & Lieber, C. M. Semiconductor nanowires. *J. Phys. D Appl. Phys.* **39**, R387 (2006).
10. Allen, M. J., Tung, V. C. & Kaner, R. B. Honeycomb carbon: a review of graphene. *Chem. Rev.* **110**, 132–145 (2009).
11. Neto, A. H. C., Guinea, F., Peres, N. M. R., Novoselov, K. S. & Geim, A. K. The electronic properties of graphene. *Rev. Mod. Phys.* **81**, 109 (2009).
12. Geim, A. K. Graphene: status and prospects. *Science* **324**, 1530–1534 (2009).
13. Butler, S. Z. et al. Progress, challenges, and opportunities in two-dimensional materials beyond graphene. *ACS Nano* **7**, 2898–2926 (2013).
14. Bhimanapati, G. R. et al. Recent advances in two-dimensional materials beyond graphene. *ACS Nano* **9**, 11509–11539 (2015).
15. Das, S., Robinson, J. A., Dubey, M., Terrones, H. & Terrones, M. Beyond graphene: progress in novel two-dimensional materials and van der Waals solids. *Annu. Rev. Mater. Res.* **45**, 1–27 (2015).
16. Ferrari, A. C. et al. Science and technology roadmap for graphene, related two-dimensional crystals, and hybrid systems. *Nanoscale* **7**, 4598–4810 (2015).
17. Castellanos-Gomez, A. Black phosphorus: narrow gap, wide applications. *J. Phys. Chem. Lett.* **6**, 4280–4291 (2015).
18. Ling, X., Wang, H., Huang, S., Xia, F. & Dresselhaus, M. S. The renaissance of black phosphorus. *Proc. Natl Acad. Sci. USA* **112**, 4523–4530 (2015).
19. Jariwala, D., Sangwan, V. K., Lauhon, L. J., Marks, T. J. & Hersam, M. C. Emerging device applications for semiconducting two-dimensional transition metal dichalcogenides. *ACS Nano* **8**, 1102–1120 (2014).
20. Ryder, C. R., Wood, J. D., Wells, S. A. & Hersam, M. C. Chemically tailoring semiconducting two-dimensional transition metal dichalcogenides and black phosphorus. *ACS Nano* **10**, 3900–3917 (2016).
21. Sangwan, V. K. & Hersam, M. C. Electronic transport in two-dimensional materials. *Annu. Rev. Phys. Chem.* **69**, 299–325 (2018).
22. Jariwala, D., Marks, T. J. & Hersam, M. C. Mixed-dimensional van der Waals heterostructures. *Nat. Mater.* **16**, 170 (2017).
23. Geim, A. K. & Grigorieva, I. V. Van der Waals heterostructures. *Nature* **499**, 419–425 (2013).
24. Mak, K. F. & Shan, J. Photonics and optoelectronics of 2D semiconductor transition metal dichalcogenides. *Nat. Photonics* **10**, 216 (2016).
25. Xia, F., Wang, H., Xiao, D., Dubey, M. & Ramasubramaniam, A. Two-dimensional material nanophotonics. *Nat. Photonics* **8**, 899 (2014).
26. Iannaccone, G., Bonaccorso, F., Colombo, L. & Fiori, G. Quantum engineering of transistors based on 2D materials heterostructures. *Nat. Nanotechnol.* **13**, 183 (2018).
27. Shi, Y., Li, H. & Li, L.-J. Recent advances in controlled synthesis of two-dimensional transition metal dichalcogenides via vapour deposition techniques. *Chem. Soc. Rev.* **44**, 2744–2756 (2015).
28. Chhowalla, M. et al. The chemistry of two-dimensional layered transition metal dichalcogenide nanosheets. *Nat. Chem.* **5**, 263–275 (2013).
29. Wang, Q. H., Kalantar-Zadeh, K., Kis, A., Coleman, J. N. & Strano, M. S. Electronics and optoelectronics of two-dimensional transition metal dichalcogenides. *Nat. Nanotechnol.* **7**, 699–712 (2012).

30. Naguib, M., Mochalin, V. N., Barsoum, M. W. & Gogotsi, Y. 25th anniversary article: MXenes: a new family of two-dimensional materials. *Adv. Mater.* **26**, 992–1005 (2014).
31. Mashtalir, O. et al. Dye adsorption and decomposition on two-dimensional titanium carbide in aqueous media. *J. Mater. Chem. A* **2**, 14334–14338 (2014).
32. Ling, X. et al. Parallel stitching of 2D materials. *Adv. Mater.* **28**, 2322–2329 (2016).
33. Wang, H. et al. Integrated circuits based on bilayer MoS2 transistors. *Nano Lett.* **12**, 4674–4680 (2012).
34. Wachter, S., Polyushkin, D. K., Bethge, O. & Mueller, T. A microprocessor based on a two-dimensional semiconductor. *Nat. Commun.* **8**, 14948 (2017).
35. Leong, W. S. & Thong, J. T. L. in *Nanotechnology (IEEE-NANO), 2015 IEEE 15th International Conference on* 534–536 https://ieeexplore.ieee.org/abstract/document/7388658/.
36. Huang, Y. et al. An innovative way of etching MoS2: characterization and mechanistic investigation. *Nano Res.* **6**, 200–207 (2013).
37. Choi, J. et al. Nanomanufacturing of 2D transition metal dichalcogenide materials using self-assembled DNA nanotubes. *Small* **11**, 5520–5527 (2015).
38. Zhou, H. et al. Thickness-dependent patterning of MoS2 sheets with well-oriented triangular pits by heating in air. *Nano Res.* **6**, 703–711 (2013).
39. Ionescu, R. et al. Oxygen etching of thick MoS 2 films. *Chem. Commun.* **50**, 11226–11229 (2014).
40. Xiao, Z., Yang, Z., Zhou, L., Zhang, L. & Wang, R. Highly conductive porous transition metal dichalcogenides via water steam etching for high-performance lithium–sulfur batteries. *ACS Appl. Mater. Interfaces* **9**, 18845–18855 (2017).
41. Han, G. G. D. et al. Photoluminescent arrays of nanopatterned monolayer MoS2. *Adv. Funct. Mater.* **27**, 1703688 (2017).
42. Yu, L. et al. Graphene/MoS2 hybrid technology for large-scale two-dimensional electronics. *Nano Lett.* **14**, 3055–3063 (2014).
43. Chen, K.-C., Chu, T.-W., Wu, C.-R., Lee, S.-C. & Lin, S.-Y. Atomic layer etchings of transition metal dichalcogenides with post healing procedures: equivalent selective etching of 2D crystal hetero-structures. *2D Mater.* **4**, 034001 (2017).
44. Zhu, H. et al. Remote plasma oxidation and atomic layer etching of MoS2. *ACS Appl. Mater. Interfaces* **8**, 19119–19126 (2016).
45. Jeon, M. H. et al. Controlled MoS2 layer etching using CF4 plasma. *Nanotechnology* **26**, 355706 (2015).
46. Nam, H. et al. MoS2 transistors fabricated via plasma-assisted nanoprinting of few-layer MoS2 flakes into large-area arrays. *ACS Nano* **7**, 5870–5881 (2013).
47. Lin, T. et al. Controlled layer-by-layer etching of MoS2. *ACS Appl. Mater. Interfaces* **7**, 15892–15897 (2015).
48. Robbins, M. C., Namgung, S., Oh, S.-H. & Koester, S. J. Cyclical thinning of black phosphorus with high spatial resolution for heterostructure devices. *ACS Appl. Mater. Interfaces* **9**, 12654–12662 (2017).
49. Kim, K. S. et al. Atomic layer etching mechanism of MoS2 for nanodevices. *ACS Appl. Mater. Interfaces* **9**, 11967–11976 (2017).
50. Lee, C. H. et al. A self-limiting layer-by-layer etching technique for 2H-MoS2. *Appl. Phys. Express* **10**, 35201 (2017).
51. Pudasaini, P. R. et al. High performance top-gated multilayer WSe2 field effect transistors. *Nanotechnology* **28**, 475202 (2017).
52. Xiao, S. et al. Atomic-layer soft plasma etching of MoS2. *Sci. Rep.* **6**, 19945 (2016).
53. Kappera, R. et al. Phase-engineered low-resistance contacts for ultrathin MoS2 transistors. *Nat. Mater.* **13**, 1128–1134 (2014).
54. Voiry, D., Mohite, A. & Chhowalla, M. Phase engineering of transition metal dichalcogenides. *Chem. Soc. Rev.* **44**, 2702–2712 (2015).
55. Cho, S. et al. Phase patterning for ohmic homojunction contact in MoTe2. *Science* **349**, 625–628 (2015).
56. Ambrosi, A., Sofer, Z. & Pumera, M. 2H→1T phase transition and hydrogen evolution activity of MoS2, MoSe2, WS2 and WSe2 strongly depends on the MX 2 composition. *Chem. Commun.* **51**, 8450–8453 (2015).
57. Ma, Y. et al. Reversible semiconducting-to-metallic phase transition in chemical vapor deposition grown monolayer WSe2 and applications for devices. *ACS Nano* **9**, 7383–7391 (2015).
58. Kappera, R. et al. Metallic 1T phase source/drain electrodes for field effect transistors from chemical vapor deposited MoS2. *Apl. Mater.* **2**, 92516 (2014).
59. Fan, X. et al. Fast and efficient preparation of exfoliated 2H MoS2 nanosheets by sonication-assisted lithium intercalation and infrared laser-induced 1T to 2H phase reversion. *Nano Lett.* **15**, 5956–5960 (2015).
60. Lin, Y.-C., Dumcenco, D. O., Huang, Y.-S. & Suenaga, K. Atomic mechanism of the semiconducting-to-metallic phase transition in single-layered MoS2. *Nat. Nanotechnol.* **9**, 391–396 (2014).
61. Katagiri, Y. et al. Gate-tunable atomically thin lateral MoS2 schottky junction patterned by electron beam. *Nano Lett.* **16**, 3788–3794 (2016).
62. Iberi, V. et al. Nanoforging single layer MoSe2 through defect engineering with focused helium ion beams. *Sci. Rep.* **6**, 30481 (2016).
63. Zhou, W. et al. Intrinsic structural defects in monolayer molybdenum disulfide. *Nano Lett.* **13**, 2615–2622 (2013).
64. Komsa, H.-P. & Krasheninnikov, A. V. Engineering the electronic properties of two-dimensional transition metal dichalcogenides by introducing mirror twin boundaries. *Adv. Electron. Mater.* https://doi.org/10.1002/aelm.201600468 (2017).
65. Coelho, P. M. et al. Post-synthesis modifications of two-dimensional MoSe2 or MoTe2 by incorporation of excess metal atoms into the crystal structure. *ACS Nano* **12**, 3975–3984 (2018).
66. Sangwan, V. K. et al. Gate-tunable memristive phenomena mediated by grain boundaries in single-layer MoS 2. *Nat. Nanotechnol.* **10**, 403 (2015).
67. Bollinger, M. V. et al. One-dimensional metallic edge states in MoS2. *Phys. Rev. Lett.* **87**, 196803 (2001).
68. Bollinger, M. V., Jacobsen, K. W. & Nørskov, J. K. Atomic and electronic structure of MoS2 nanoparticles. *Phys. Rev. B* **67**, 085410 (2003).
69. Pan, H. & Zhang, Y.-W. Edge-dependent structural, electronic and magnetic properties of MoS2 nanoribbons. *J. Mater. Chem.* **22**, 7280 (2012).
70. Botello-Méndez, A. R., López-Urías, F., Terrones, M. & Terrones, H. Metallic and ferromagnetic edges in molybdenum disulfide nanoribbons. *Nanotechnology* **20**, 325703 (2009).
71. Mahjouri-Samani, M. et al. Tailoring vacancies far beyond intrinsic levels changes the carrier type and optical response in monolayer MoSe2−x crystals. *Nano Lett.* **16**, 5213–5220 (2016).
72. Komsa, H.-P. et al. Two-dimensional transition metal dichalcogenides under electron irradiation: defect production and doping. *Phys. Rev. Lett.* **109**, 035503 (2012).
73. Komsa, H.-P., Kurasch, S., Lehtinen, O., Kaiser, U., & Krasheninnikov, A. V. From point to extended defects in two-dimensional MoS2: evolution of atomic structure under electron irradiation. *Phys. Rev. B* **88**, 035301 (2013).
74. Fox, D. S. et al. Nanopatterning and electrical tuning of MoS2 layers with a subnanometer helium ion beam. *Nano Lett.* **15**, 5307–5313 (2015).
75. Stanford, M. G. et al. Focused helium-ion beam irradiation effects on electrical transport properties of few-layer WSe2: enabling nanoscale direct write homojunctions. *Sci. Rep.* **6**, 27276 (2016).
76. Stanford, M. G. et al. Tungsten diselenide patterning and nanoribbon formation by gas-assisted focused helium ion beam induced etching. *Small Methods* **1**, 1600060 (2017).
77. Stanford, M. G. et al. High conduction hopping behavior induced in transition metal dichalcogenides by percolating defect networks: toward atomically thin circuits. *Adv. Funct. Mater.* **27**, 1702829 (2017).
78. Ghorbani-Asl, M., Kretschmer, S., Spearot, D. E. & Krasheninnikov, A. V. Two-dimensional MoS2 under ion irradiation: from controlled defect production to electronic structure engineering. *2D Mater.* **4**, 025078 (2017).
79. Dyck, O. et al. Assembling di-and multiatomic si clusters in graphene via electron beam manipulation. Preprint at https://arxiv.org/abs/1710.09416 (2017).
80. Chow, P. K. et al. Defect-induced photoluminescence in monolayer semiconducting transition metal dichalcogenides. *ACS Nano* **9**, 1520–1527 (2015).
81. Lu, A.-Y. et al. Janus monolayers of transition metal dichalcogenides. *Nat. Nanotechnol.* **12**, 744 (2017).
82. Jadwiszczak, J. et al. Oxide-mediated self-limiting recovery of field effect mobility in plasma-treated MoS2. *Sci. Adv.* **4**, eaao5031 (2017).
83. Tongay, S. et al. Defects activated photoluminescence in two-dimensional semiconductors: interplay between bound, charged, and free excitons. *Sci. Rep.* **3**, 2657 (2013).
84. Ma, L. et al. Tailoring the optical properties of atomically-thin WS2 via ion irradiation. *Nanoscale* **9**, 11027–11034 (2017).
85. Yuan, S., Rudenko, A. N. & Katsnelson, M. I. Transport and optical properties of single-and bilayer black phosphorus with defects. *Phys. Rev. B* **91**, 115436 (2015).
86. Addou, R. et al. One dimensional metallic edges in atomically thin WSe2 induced by air exposure. *2D Mater.* **5**, 025017 (2018).
87. Pomerantseva, E. & Gogotsi, Y. Two-dimensional heterostructures for energy storage. *Nat. Energy* **2**, 17089 (2017).
88. Suh, J. et al. Doping against the native propensity of MoS2: degenerate hole doping by cation substitution. *Nano Lett.* **14**, 6976–6982 (2014).
89. Zhang, K. et al. Tuning the electronic and photonic properties of monolayer MoS2 via in situ rhenium substitutional doping. *Adv. Funct. Mater.* **28**, 1706950 (2018).
90. Khondaker, S. I. & Islam, M. R. Bandgap engineering of MoS2 flakes via oxygen plasma: a layer dependent study. *J. Phys. Chem. C* **120**, 13801–13806 (2016).
91. Azcatl, A. et al. Covalent nitrogen doping and compressive strain in MoS_2 by remote N_2 plasma exposure. *Nano Lett.* **16**, 5437–5443 (2016).
92. Chen, M. et al. Stable few-layer MoS2 rectifying diodes formed by plasma-assisted doping. *Appl. Phys. Lett.* **103**, 142110 (2013).
93. Tosun, M. et al. Air-stable n-doping of WSe 2 by anion vacancy formation with mild plasma treatment. *ACS Nano* **10**, 6853–6860 (2016).

94. Sarkar, D. et al. Functionalization of transition metal dichalcogenides with metallic nanoparticles: implications for doping and gas-sensing. *Nano Lett.* **15**, 2852–2862 (2015).
95. Bhanu, U., Islam, M. R., Tetard, L. & Khondaker, S. I. Photoluminescence quenching in gold-MoS2 hybrid nanoflakes. *Sci. Rep.* **4**, 5575 (2014).
96. Mouri, S., Miyauchi, Y. & Matsuda, K. Tunable photoluminescence of monolayer MoS2 via chemical doping. *Nano Lett.* **13**, 5944–5948 (2013).
97. Yang, L. et al. Chloride molecular doping technique on 2D materials: WS2 and MoS2. *Nano Lett.* **14**, 6275–6280 (2014).
98. Kiriya, D., Tosun, M., Zhao, P., Kang, J. S. & Javey, A. Air-stable surface charge transfer doping of MoS2 by benzyl viologen. *J. Am. Chem. Soc.* **136**, 7853–7856 (2014).
99. Gong, Y. et al. Spatially controlled doping of two-dimensional SnS2 through intercalation for electronics. *Nat. Nanotechnol.* **13**, 294–299 (2018).
100. Zhao, M. et al. Large-scale chemical assembly of atomically thin transistors and circuits. *Nat. Nanotechnol.* **11**, 954 (2016).
101. Guimara~es, M. H. D. et al. Atomically thin ohmic edge contacts between two-dimensional materials. *ACS Nano* **10**, 6392–6399 (2016).
102. Liu, L. et al. Heteroepitaxial growth of two-dimensional hexagonal boron nitride templated by graphene edges. *Science* **343**, 163–167 (2014).
103. Li, M.-Y. et al. Epitaxial growth of a monolayer WSe2-MoS2 lateral pn junction with an atomically sharp interface. *Science* **349**, 524–528 (2015).
104. Sahoo, P. K., Memaran, S., Xin, Y., Balicas, L. & Gutiérrez, H. R. One-pot growth of two-dimensional lateral heterostructures via sequential edge-epitaxy. *Nature* **553**, 63 (2018).
105. Chen, K. et al. Electronic properties of MoS2–WS2 heterostructures synthesized with two-step lateral epitaxial strategy. *ACS Nano* **9**, 9868–9876 (2015).
106. Heo, H. et al. Rotation-misfit-free heteroepitaxial stacking and stitching growth of hexagonal transition-metal dichalcogenide monolayers by nucleation kinetics controls. *Adv. Mater.* **27**, 3803–3810 (2015).
107. Xie, S. et al. Coherent atomically-thin superlattices with engineered strain. Preprint at https://scirate.com/arxiv/1708.09539 (2017).
108. Zhang, X.-Q., Lin, C.-H., Tseng, Y.-W., Huang, K.-H. & Lee, Y.-H. Synthesis of lateral heterostructures of semiconducting atomic layers. *Nano Lett.* **15**, 410–415 (2014).
109. Gong, Y. et al. Two-step growth of two-dimensional WSe2/MoSe2 heterostructures. *Nano Lett.* **15**, 6135–6141 (2015).
110. Bogaert, K. et al. Diffusion-mediated synthesis of MoS2/WS2 lateral heterostructures. *Nano Lett.* **16**, 5129–5134 (2016).
111. Gong, Y. et al. Vertical and in-plane heterostructures from WS2/MoS2 monolayers. *Nat. Mater.* **13**, 1135–1142 (2014).
112. Huang, C. et al. Lateral heterojunctions within monolayer MoSe2–WSe2 semiconductors. *Nat. Mater.* **13**, 1096–1101 (2014).
113. Zhang, Z. et al. Robust epitaxial growth of two-dimensional heterostructures, multiheterostructures, and superlattices. *Science* **357**, 788–792 (2017).
114. Han, Y. et al. Sub-nanometre channels embedded in two-dimensional materials. *Nat. Mater.* **17**, 129 (2018).
115. Jariwala, D., Davoyan, A. R., Wong, J. & Atwater, H. A. Van der Waals materials for atomically-thin photovoltaics: promise and outlook. *ACS Photonics* **4**, 2962–2970 (2017).
116. Mahjouri-Samani, M. et al. Patterned arrays of lateral heterojunctions within monolayer two-dimensional semiconductors. *Nat. Commun.* **6**, 7749 (2015).
117. Choudhary, N. et al. Two-dimensional lateral heterojunction through bandgap engineering of MoS 2 via oxygen plasma. *J. Phys. Condens. Matter* **28**, 364002 (2016).
118. Dyck, O., Kim, S., Kalinin, S. V. & Jesse, S. Placing single atoms in graphene with a scanning transmission electron microscope. *Appl. Phys. Lett.* **111**, 113104 (2017).
119. Kalinin, S. V., Borisevich, A. & Jesse, S. Fire up the atom forge. *Nat. News* **539**, 485 (2016).
120. Susi, T., Meyer, J. C. & Kotakoski, J. Manipulating low-dimensional materials down to the level of single atoms with electron irradiation. *Ultramicroscopy* **180**, 163–172 (2017).
121. Jesse, S. et al. Directing matter: toward atomic-scale 3D nanofabrication. *ACS Nano* **10**, 5600–5618 (2016).
122. Masih Das, P. et al. Controlled sculpture of black phosphorus nanoribbons. *ACS Nano* **10**, 5687–5695 (2016).
123. Liu, X. et al. Top–down fabrication of sub-nanometre semiconducting nanoribbons derived from molybdenum disulfide sheets. *Nat. Commun.* **4**, 1776 (2013).
124. Urbanos, F. J. et al. in *Nanoengineering: Fabrication, Properties, Optics, and Devices XIV* 10354, 103540G Rome, Italy (International Society for Optics and Photonics, 2017).
125. Li, H. et al. Laterally stitched heterostructures of transition metal dichalcogenide: chemical vapor deposition growth on lithographically patterned area. *ACS Nano* **10**, 10516–10523 (2016).
126. Kim, S. et al. Multi-purposed Ar gas cluster ion beam processing for graphene engineering. *Carbon* **131**, 142–148 (2018).
127. Wu, J.-B. et al. Monolayer molybdenum disulfide nanoribbons with high optical anisotropy. *Adv. Opt. Mater.* **4**, 756–762 (2016).
128. Abbas, A. N. et al. Patterning, characterization, and chemical sensing applications of graphene nanoribbon arrays down to 5 nm using helium ion beam lithography. *ACS Nano* **8**, 1538–1546 (2014).
129. Livengood, R. H., Greenzweig, Y., Liang, T. & Grumski, M. Helium ion microscope invansiveness and image study for semiconductor applications. *J. Vac. Sci. Technol. B* **25**, 2547 (2007).
130. Stanford, M. G. et al. In situ mitigation of subsurface and peripheral focused ion beam damage via simultaneous pulsed laser heating. *Small* **12**, 1779–1787 (2016).
131. Ataca, C., S¸ahin, H., Aktu¨rk, E. & Ciraci, S. Mechanical and electronic properties of MoS2 nanoribbons and their defects. *J. Phys. Chem. C* **115**, 3934–3941 (2011).
132. Botello-Méndez, A. R., López-Urías, F., Terrones, M. & Terrones, H. Metallic and ferromagnetic edges in molybdenum disulfide nanoribbons. *Nanotechnology* **20**, 325703 (2009).
133. Rani, R. et al. Controlled formation of nanostructures on MoS2 layers by focused laser irradiation. *Appl. Phys. Lett.* **110**, 83101 (2017).
134. Kim, S. W. et al. Patterning of periodic ripples in monolayer MoS2 by using laser irradiation. *J. Korean Phys. Soc.* **69**, 1505–1508 (2016).
135. Bissett, M. A., Hattle, A. G., Marsden, A. J., Kinloch, I. A. & Dryfe, R. A. W. Enhanced photoluminescence of solution-exfoliated transition metal dichalcogenides by laser etching. *ACS Omega* **2**, 738–745 (2017).
136. Cao, L. et al. Direct laser-patterned micro-supercapacitors from paintable MoS2 films. *Small* **9**, 2905–2910 (2013).
137. Lin, J. et al. Laser-induced porous graphene films from commercial polymers. *Nat. Commun.* **5**, 5714 (2014).
138. Peng, Z., Lin, J., Ye, R., Samuel, E. L. G. & Tour, J. M. Flexible and stackable laser-induced graphene supercapacitors. *ACS Appl. Mater. Interfaces* **7**, 3414–3419 (2015).
139. Lu, J. et al. Bandgap engineering of phosphorene by laser oxidation toward functional 2D materials. *ACS Nano* **9**, 10411–10421 (2015).
140. Castellanos-Gomez, A. et al. Laser-thinning of MoS2: on demand generation of a single-layer semiconductor. *Nano Lett.* **12**, 3187–3192 (2012).
141. Delawski, E. & Parkinson, B. A. Layer-by-layer etching of two-dimensional metal chalcogenides with the atomic force microscope. *J. Am. Chem. Soc.* **114**, 1661–1667 (1992).
142. Liu, X. et al. Scanning probe nanopatterning and layer-by-layer thinning of black phosphorus. *Adv. Mater.* **29**, 1604121 (2017).
143. Dago, A. I., Ryu, Y. K. & Garcia, R. Sub-20 nm patterning of thin layer WSe2 by scanning probe lithography. *Appl. Phys. Lett.* **109**, 163103 (2016).
144. Zhang, C. J. et al. Stamping of flexible, coplanar micro-supercapacitors using MXene inks. *Adv. Funct. Mater.* **28**, 1705506 (2018).
145. Hung, Y.-H. et al. Scalable patterning of MoS2 nanoribbons by micromolding in capillaries. *ACS Appl. Mater. Interfaces* **8**, 20993–21001 (2016).
146. Martella, C. et al. Anisotropic MoS2 nanosheets grown on self-organized nanopatterned substrates. *Adv. Mater.* **29**, 1605785 (2017).
147. Martella, C. et al. Designer shape anisotropy on transition-metal-dichalcogenide nanosheets. *Adv. Mater.* **30**, 1705615 (2018).
148. Jang, S. et al. Highly periodic metal dichalcogenide nanostructures with complex shapes, high resolution, and high aspect ratios. *Adv. Funct. Mater.* **27**, 1703842 (2017).
149. Nourbakhsh, A. et al. MoS2 field-effect transistor with sub-10 nm channel length. *Nano Lett.* **16**, 7798–7806 (2016).
150. Choi, J. et al. Nanomanufacturing of 2D transition metal dichalcogenide materials using self-assembled DNA nanotubes. *Small* **11**, 5520–5527 (2015).
151. Ju, L. et al. Graphene plasmonics for tunable terahertz metamaterials. *Nat. Nanotechnol.* **6**, 630 (2011).
152. Brar, V. W., Jang, M. S., Sherrott, M., Lopez, J. J. & Atwater, H. A. Highly confined tunable mid-infrared plasmonics in graphene nanoresonators. *Nano Lett.* **13**, 2541–2547 (2013).
153. Liu, Z. & Aydin, K. Localized surface plasmons in nanostructured monolayer black phosphorus. *Nano Lett.* **16**, 3457–3462 (2016).
154. Low, T. et al. Plasmons and screening in monolayer and multilayer black phosphorus. *Phys. Rev. Lett.* **113**, 106802 (2014).
155. Whitney, W. S. et al. Field effect optoelectronic modulation of quantum-confined carriers in black phosphorus. *Nano Lett.* **17**, 78–84 (2016).
156. Quereda, J. et al. Strong modulation of optical properties in black phosphorus through strain-engineered rippling. *Nano Lett.* **16**, 2931–2937 (2016).
157. Feng, J., Qian, X., Huang, C.-W. & Li, J. Strain-engineered artificial atom as a broad-spectrum solar energy funnel. *Nat. Photonics* **6**, 866 (2012).
158. Palacios-Berraquero, C. et al. Large-scale quantum-emitter arrays in atomically thin semiconductors. *Nat. Commun.* **8**, 15093 (2017).

159. Kumar, S., Kaczmarczyk, A. & Gerardot, B. D. Strain-induced spatial and spectral isolation of quantum emitters in mono-and bilayer WSe2. *Nano Lett.* **15**, 7567–7573 (2015).
160. Jariwala, D. Tunable confinement of charges and excitations. *Nat. Nanotechnol.* **13**, 99–100 (2018).
161. Wang, K. et al. Electrical control of charged carriers and excitons in atomically thin materials. *Nat. Nanotechnol.* **13**, 128–132 (2018).
162. Wei, G. et al. Size-tunable lateral confinement in monolayer semiconductors. *Sci. Rep.* **7**, 3324 (2017).
163. Xu, K. et al. Sub-10 nm nanopattern architecture for 2D material field-effect transistors. *Nano Lett.* **17**, 1065–1070 (2017).
164. Miao, J., Zhang, S., Cai, L., Scherr, M. & Wang, C. Ultrashort channel length black phosphorus field-effect transistors. *ACS Nano* **9**, 9236–9243 (2015).
165. Xie, S. et al. Coherent, atomically thin transition-metal dichalcogenide superlattices with engineered strain. *Science* **359**, 1131–1136 (2018).